VOLUME 31 1953

Canadian Journal of Technology

Published by THE NATIONAL RESEARCH COUNCIL
OTTAWA CANADA

VOLUME 31 JANUARY 1953 NUMBER 1

Canadian Journal of Technology

Editor: G. A. LEDINGHAM

Published by THE NATIONAL RESEARCH COUNCIL
OTTAWA CANADA

CANADIAN JOURNAL OF TECHNOLOGY

(Formerly Section F, Canadian Journal of Research)

The CANADIAN JOURNAL OF TECHNOLOGY is published monthly by the National Research Council of Canada under the authority of the Chairman of the Committee of the Privy Council on Scientific and Industrial Research. Matters of general policy are the responsibility of a joint Editorial Board consisting of members of the National Research Council of Canada and the Royal Society of Canada.

The National Research Council of Canada publishes also: *Canadian Journal of Botany, Canadian Journal of Chemistry, Canadian Journal of Medical Sciences, Canadian Journal of Physics, Canadian Journal of Zoology.*

The CANADIAN JOURNAL OF TECHNOLOGY and the CANADIAN JOURNAL OF CHEMISTRY have been chosen by the Chemical Institute of Canada as its medium of publication for scientific papers.

EDITORIAL BOARD

Manuscripts should be addressed to:

DR. LÉO MARION,
Editor-in-Chief,
Canadian Journal of Technology,
National Research Council,
Ottawa, Canada.

Each manuscript should be typewritten, double-spaced, and the original and one extra copy submitted (see **Notice to Contributors** inside of back cover).

Subscriptions, renewals, and orders for back numbers should be addressed to:

Administrative Services,
National Research Council,
Ottawa, Canada.

Subscription-rate: $4.00 a year; single numbers: 50 cents. Special rates can be obtained for subscriptions to more than one of the Journals published by the National Research Council.

Engin
direct

Canadian Journal of Technology

Issued by THE NATIONAL RESEARCH COUNCIL OF CANADA

VOLUME 31 JANUARY, 1953 NUMBER 1

SOME FACTORS AFFECTING THE FERMENTATION OF BEET MOLASSES BY *PSEUDOMONAS HYDROPHILA*[1]

BY P. A. ANASTASSIADIS[2] AND J. A. WHEAT[3]

ABSTRACT

The production of 2, 3-butanediol by fermentation of beet molasses with one strain of *Pseudomonas hydrophila* has been investigated on a laboratory scale to obtain data necessary for larger scale fermentations. Tests were carried out at various sugar concentrations (5 – 12.5%) and pH levels (3.5 – 8.0) with and without additives. Dibasic ammonium phosphate and corn steep liquor increased the initial rate of the fermentation and the uniformity of the results but only corn steep liquor increased the final diol yield. Of the initial sugar concentrations tested, the highest that gave rapid and complete dissimilation of the sugar was 7.5%. Acetic and sulphuric acids were found to be suitable for adjusting the initial pH of the medium and highest yields were obtained with an initial pH of 6.0. Varying the amount of inoculum from 0.1 to 1.0% had no effect on diol yield or rate of fermentation. Fermentation of molasses solutions containing 7.5% sugar and 0.05% corn steep liquor gave an average yield in 40 hr. of 78.2 moles of butanediol and 42.5 moles of ethanol per 100 moles of sugar added.

INTRODUCTION

Murphy *et al.* (3) have reported studies on the 2, 3-butanediol fermentation of beet molasses by strains of *Pseudomonas hydrophila*. In the majority of their experiments they used molasses diluted to 5% sucrose and supplemented with 0.11% dibasic ammonium phosphate and 0.11% bran. Other experiments were made with higher sugar concentrations and proportionately higher concentrations of the supplements. A comparison of *P. hydrophila* with a high yielding strain of *Aerobacter aerogenes*, showed that the former gave higher yields of diol with correspondingly lower yields of ethanol.

Murphy, Stranks, and Harmsen (2) studied the nutritive requirements of *Bacillus polymyxa*, *Aerobacter aerogenes*, *Bacillus subtilis*, and *Serratia marcescens* for the fermentation of beet molasses. Their results showed that beet molasses, although high in total phosphorus, was deficient in available phosphorus but was an excellent raw material for the 2, 3-butanediol fermentation, provided sufficient soluble orthophosphate salts were added. Stimulation of bacterial growth and fermentation by phosphate was most effective in the early stages of the fermentation and, although added phosphate usually caused an increase in diol yield, sometimes the final yield was not affected. The

[1] *Manuscript received August 25, 1952.*
Contribution from the Division of Applied Biology, National Research Laboratories, Ottawa, Canada. Issued as Paper No. 143 on the Uses of Plant Products and as N.R.C. No. 2872.

[2] *Agronomist, Industrial Utilization Investigations. Present address: Department of Chemistry, Macdonald College, Macdonald College, Que.*
[3] *Chemical Engineer, Industrial Utilization Investigations.*

addition of organic stimulants to a medium containing phosphate resulted in fermentations with initial rates and final yields slightly higher than those obtained with phosphate alone.

The aim of the present investigation was to obtain additional information about some of the factors affecting the fermentation of beet molasses by *P. hydrophila* and to determine optimum conditions for use with larger scale fermentations.

MATERIALS AND METHODS

Beet molasses (crop year 1949), which contained 51.7% sugar calculated as invert sugar, was obtained from the Canada and Dominion Sugar Co., Ltd., Chatham, Ont. Media were prepared by diluting a weighed amount of molasses and additives to a sugar concentration of 7.49% by weight or 7.81 gm. per 100 ml. This sugar concentration was selected as optimal on the basis of the work of Murphy *et al.* (3). The pH was then adjusted and 100 ml. aliquots were dispensed into 500 ml. Erlenmeyer flasks and sterilized at 15 p.s.i. for 15 min. as recommended by Simpson and Stranks (5) for fermentation of beet molasses by *Bacillus polymyxa*. During sterilization there was an increase in pH, which was determined in flasks set up for this purpose. It was found to be about 0.3 – 0.4 for a solution set at pH 5.5 prior to sterilization with either acetic or sulphuric acid, and about 0.5 for a solution set at pH 6.5. Throughout this paper the initial pH reported is that of the medium before autoclaving.

After inoculation, the flasks were incubated at 32 – 34°C. on a rotary shaker operated at 100 r.p.m. Sufficient flasks were started so that at various times throughout the fermentations pairs could be removed for analysis.

P. hydrophila N.R.C. 492 (3) was used throughout the investigation. Inocula were prepared by transferring the culture from 24 hr. molasses agar slants to 500 ml. Erlenmeyer flasks containing 100 ml. of a 10% molasses and 0.5% yeast extract medium adjusted to pH 5.5 with acetic acid prior to autoclaving. After 24 hr. incubation on the shaker, 1.0 ml. of inoculum was pipetted into each of the fermentation flasks. This procedure was used for all experiments except where otherwise noted.

The analytical methods of Neish (4) were used, with some modification, for 2, 3-butanediol and ethanol. Ethanol results were not corrected for the diol and acetoin that distilled over with the ethanol. Nor were butanediol results corrected for acetoin and, throughout the paper, diol yields should be understood to be diol plus acetoin. Yields are reported as gm. per 100 ml. of medium except where otherwise noted. The sugar content of the molasses was determined by the Lane-Eynon method (6). Average pH values were calculated directly from individual pH measurements without conversion to hydrogen ion activities.

EXPERIMENTAL RESULTS AND CONCLUSIONS

Adjustment of pH

An initial experiment on the effect of pH on diol yield was carried out in a molasses medium with no additives, adjusted with acetic acid to pH levels

ranging from 3.5 to 8.0 in 0.5 increments. At pH 6.0 and above, the yields were approximately equal and it was found that by 16 hr., the pH of all flasks had decreased to the same level. At pH 5.5 the yield was slightly less than at the higher levels while at pH 5.0 and below there was no fermentation.

The effect of initial pH was again tested using either acetic or sulphuric acid with media containing 0.05% corn steep liquor (C.S.L.). The pH range was narrowed to include only pH 5.5, 6.0, and 6.5. Results are given in Table I

TABLE I

EFFECT ON FERMENTATION OF ADJUSTING WITH DIFFERENT ACIDS TO VARIOUS pH LEVELS
(Standard inoculation; 40 hr. incubation; 0.05% added C.S.L.)

	Acid					
	Acetic			Sulphuric		
	Initial pH					
	5.5	6.0	6.5	5.5	6.0	6.5
Diol plus acetoin, gm. per 100 ml.	3.15	3.22	3.08	3.12	3.16	2.94
Standard deviation	0.04	0.04	—	0.05	0.03	—
No. of flasks	12	10	2	10	8	2

for all available data derived under the conditions specified. The differences in yield between media adjusted with acetic acid and sulphuric acid at pH levels of 5.5 and 6.0 were statistically significant, but not highly so (probability of 0.05 at pH 5.5 and 0.01 at 6.0). Although both acids were satisfactory for pH adjustment, the slightly higher yield with acetic led to its use in subsequent experiments.

The results of Table I indicate that the diol yields at pH 6.5 were lower than at the other pH levels and, consequently, this pH was not studied further. Yields obtained at pH levels of 5.5 and 6.0 are compared in Table II for media

TABLE II

EFFECT OF INITIAL pH AND NUTRIENTS ON FERMENTATION
(Standard inoculation; 40 hr. incubation)

	Initial pH					
	5.5			6.0		
	Additive					
	None	0.01% P_2O_5	0.05% C.S.L.	None	0.01% P_2O_5	0.05% C.S.L.
Diol plus acetoin, gm. per 100 ml.	2.52	2.72	3.15	2.88	2.84	3.22
Standard deviation	0.64	0.10	0.04	0.42	0.10	0.04
No. of flasks	14	12	12	8	12	10

containing no additives, 0.01% P_2O_5 added as dibasic ammonium phospnate, and 0.05% C.S.L. With no additive, the difference between yields at the two pH levels was not significant. With either additive, the yield at an initial pH of 6.0 was significantly higher than at 5.5.

The variation of pH throughout the fermentation is shown in Table III. These values were obtained with media adjusted to pH 6.0 prior to sterilization. The results show that with the addition of phosphate there was a lower pH throughout the fermentation than with C.S.L. or with no supplement.

TABLE III

VARIATION OF pH DURING THE FERMENTATION

(Standard inoculation; initial pH 6.0; number of flasks in parentheses)

Time, hr. \ Additive	None	0.01% P_2O_5	0.05% C.S.L.
16	6.5 (8)	5.6 (10)	6.3 (4)
24	6.3 (8)	5.6 (10)	6.0 (4)
40	6.0 (8)	5.4 (12)	6.1 (10)

Effect of Molasses Dilution

The optimum sugar concentration for a fermentation process is the highest that will give rapid and complete dissimilation of the sugar with a high product yield. Data obtained at four sugar concentrations with proportional concentrations of P_2O_5 added as dibasic ammonium phosphate are presented in Table IV. Because of volume changes during autoclaving and fermentations, yields are not reported as gm. per 100 gm. of sugar. The values given, however, are reliable indices of relative yields. Of the concentrations tested, 7.5% was the optimum and was used for all other experiments.

TABLE IV

EFFECT OF MOLASSES DILUTION ON YIELD OF DIOL PLUS ACETOIN

(Inoculum adjusted to pH 6.0 and used at 8 hr.; initial pH 6.0; yield expressed as (gm. per 100 ml.) (100)/initial sugar concentration, %; number of flasks, 2)

Time, hr.	Concentration of sugar			
	5.0	7.5	10.0	12.5
	Added P_2O_5, %			
	0.0067	0.0100	0.0133	0.0167
16	25.6	24.9	22.6	17.5
24	36.0	36.0	27.9	21.4
32	36.0	36.8	30.7	24.2
40	36.2	37.2	33.8	26.6
48	37.4	37.8	35.9	28.2

Effect of Added Phosphate

Added dibasic ammonium phosphate up to a concentration of 0.01% P_2O_5 caused no change in the final yield of diol but, above this concentration, it caused a slight decrease (Table V). Added phosphate did, however, markedly increase the initial rate of fermentation. The maximum rate over the first 16

TABLE V

EFFECT OF PHOSPHATE CONCENTRATION ON YIELD OF DIOL PLUS ACETOIN

(Standard inoculation; phosphate added as $(NH_4)_2HPO_4$; initial pH, 6.0; number of flasks, 2; yield expressed as gm. per 100 ml.)

Added P_2O_5, % \ Time, hr.	16	24	32	40
0	1.1	1.9	2.4	3.1
0.001	1.4	2.2	2.7	3.1
0.005	2.4	3.0	3.0	3.1
0.01	2.4	2.6	2.9	3.0
0.02	2.0	2.4	2.6	2.7
0.06	2.1	2.4	2.6	2.7

hr. occurred at concentrations of 0.005% and 0.01% P_2O_5, with essentially no difference between the rates at these two phosphate levels. In preliminary larger scale tests, fermentations with 0.01% P_2O_5 were complete in 48 hr. whereas those with 0.005% P_2O_5 required 60 hr. The higher concentration of added phosphate was therefore selected for further tests.

Table II shows average results obtained with 0.01% P_2O_5 at pH levels of 5.5 and 6.0. At both pH levels the diol yield with added phosphate was not significantly different from the yield without added phosphate. Added phosphate, however, did increase the uniformity of the results as shown by the lower standard deviations.

When triple superphosphate was used as an alternative phosphate source, diol yields were lower than those obtained with no additive (Table VI). Hence, this additive was not studied further.

TABLE VI

EFFECT OF TRIPLE SUPERPHOSPHATE ON YIELD OF DIOL PLUS ACETOIN

(Standard inoculation; initial pH, 5.5; 40 hr. incubation; number of flasks, 2)

Added P_2O_5, %	Yield, gm. per 100 ml.
0	2.52*
0.01	2.3
0.05	2.5
0.10	2.2
0.50	0.1

**Average of 14 flasks.*

Effect of Added Corn Steep Liquor

Added corn steep liquor at concentrations of 0.2% and below had no effect on the final yield of diol while concentrations above 0.6% decreased the final yield (Table VII). Although maximum fermentation rates were obtained with 0.2 and 0.6% C.S.L., more extensive tests with 0.05% had been made before the data of Table VII were available.

TABLE VII

EFFECT OF CORN STEEP LIQUOR ON YIELD OF DIOL PLUS ACETOIN
(Standard inoculation; initial pH, 6.0; number of flasks, 2; yield expressed as gm. per 100 ml.)

Time, hr. / C.S.L., %	16	24	32	40
0	1.1	1.9	2.3	3.0
0.01	1.2	1.9	2.4	2.8
0.02	1.3	2.0	2.5	3.2
0.05	1.4	2.2	2.7	3.2
0.07	1.5	2.3	2.8	3.2
0.10	1.6	2.5	2.9	3.1
0.20	1.9	2.9	3.1	3.1
0.60*	2.3	2.8	3.1	2.8
1.0*	1.9	2.4	2.6	2.6
2.0*	1.7	1.8	2.0	2.2

**Only one flask at these concentrations of C.S.L.*

Average results with 0.05% C.S.L. are presented in Table II where they may be compared with the data obtained with no supplement and with added phosphate. At both initial pH levels, the diol yields with 0.05% C.S.L. were significantly higher than the yields obtained with 0.01% P_2O_5 or with no additive. The standard deviations with C.S.L. were even lower than with added phosphate.

Investigation of Inoculum

Results with three inoculum media, 10% molasses with 0.005% P_2O_5, 0.01% P_2O_5, or 0.5% yeast extract, are given in Table VIII. The media (initial pH 6.0) were incubated in the same manner as the fermentation flasks but instead of being used as inoculum they were removed for analysis at the times shown. Instead of inoculating these flasks by transferring the culture from a slant with a wire loop (a method subject to large variation in the number of organisms transferred), the culture was washed from a slant with 2 ml. of medium and 0.3 ml. of the suspension was pipetted into each of the test flasks. If it is assumed that inocula should be used while they are in the logarithmic growth phase and that diol production in this phase is proportional to the number of bacterial cells (1), the data indicate that the phosphate media should be used at 12 – 16 hr. and that the yeast extract medium should be used before 12

hr. Repetition of this experiment with media set at an initial pH of 5.5 gave essentially the same results. Following these experiments, the yeast extract inoculum was arbitrarily adjusted to pH 6.0 instead of 5.5 and used after eight hours' incubation, instead of after 24. However, there was no noticeable improvement in fermentation rate or yield.

TABLE VIII

FERMENTATION OF INOCULUM MEDIA

(10% molasses; see text for method of inoculating; initial pH, 6.0; number of flasks, 2; yield expressed as gm. per 100 ml.

Additive / Time, hr.	0.005% P_2O_5	0.01% P_2O_5	0.5% Y.E.*
12	0.9	0.4	1.6
16	1.7	1.8	2.1
20	2.0	2.0	2.1
24	2.0	2.1	2.1

**Yeast extract.*

When the amount of inoculum was varied from 0.1 to 1.0% there was no appreciable difference in final diol yield nor in fermentation rate. In this experiment the fermentation medium was adjusted to an initial pH of 6.0 and contained 0.01% added P_2O_5.

Fermentation Yields

Fermentation yields calculated as moles of product per 100 moles of sugar added are given in Table IX. To make the computation, the density of initial and final media were taken as 1.042 and 1.018 gm. per ml., respectively. These are average values for pilot plant mashes of the same concentration. The evaporation loss on autoclaving was found to be 3.5%. It was assumed that carbon dioxide evolution during the fermentation accounted for a loss of weight of one-half the sugar added. In Table IX, the sum of diol plus acetoin plus one-half the ethanol yield is a measure of the efficiency of the fermentation.

TABLE IX

FERMENTATION YIELDS ON BASIS OF SUGAR ADDED

(Yields calculated from the data of Table II for pH 6.0 and expressed as moles per 100 moles of invert sugar)

Additive	None	0.01% P_2O_5	0.05% C.S.L.
Diol + acetoin	70.1	69.1	78.2
Ethanol	38.5	48.8	42.5
Diol + acetoin + ½ ethanol	89.4	93.5	99.4

DISCUSSION

The optimum sugar concentration of 7.5% found in this work is in agreement with the results of Murphy *et al.* (3) but is higher than the optimum found by Simpson and Stranks (5) for fermentation by *B. polymyxa*. Added phosphate gave essentially the same results with *P. hydrophila* as Murphy, Stranks, and Harmsen (2) obtained with four other species of bacteria except that these authors reported a frequent increase in final yield when phosphate was added. This difference could have been caused by the different species or it is possible that low yields were obtained with added phosphate in the present investigation because of the low pH throughout the fermentation with this additive. The increased yield with C.S.L. supports the conclusion of Murphy, Stranks, and Harmsen that beet molasses is deficient in some organic factor as well as available phosphate.

Although added phosphate did not increase the final diol yield it was beneficial in that it increased the initial rate of fermentation and gave more uniform results. The increased initial rate, even though it did not shorten the time of fermentation, would afford a better chance of overcoming contamination in larger scale fermentations.

In this investigation, the fermentation efficiency with 0.05% C.S.L. was the same as that obtained by Murphy *et al.* (3) with 0.054% P_2O_5 and 0.10% bran. Unreported results on the effect of bran were very similar to those with corn steep liquor; the addition of 0.10% bran gave approximately the same product yield and fermentation rate as 0.07% C.S.L. The use of bran would not be recommended for commercial operation because the bran particles would have to be screened out before recovering the products.

Although the effect of aeration was not studied in this investigation, it is evident from previous laboratory results (5) that effective aeration is required to obtain a high ratio of diol plus acetoin to ethanol.

REFERENCES

1. Blackwood, A. C. and Ledingham, G. A. Can. J. Research, F, 25: 180–191. 1947.
2. Murphy, D., Stranks, D. W., and Harmsen, G. W. Can. J. Technol. 29: 131–143. 1951.
3. Murphy, D., Watson, R. W., Muirhead, D. R., and Barnwell, J. L. Can. J. Technol. 29: 375–381. 1951.
4. Neish, A.C. Report No. 46-8-3. Division of Applied Biology, National Research Council of Canada, Ottawa, June 1946.
5. Simpson, F. J. and Stranks, D. W. Can. J. Technol. 29: 87–97. 1951.
6. Skinner, W. W. Methods of analysis of the association of official agricultural chemists. 4th ed. Washington, D.C. 1935.

RECEIVING PROPERTIES OF A WIRE LOOP WITH A SPHEROIDAL CORE[1]

By James R. Wait

ABSTRACT

The relative gain of a low frequency loop antenna is calculated for a spheroidal shaped core. The cases considered are where the loop axis is coaxial and where it is at right angles to the spheroid axis of symmetry. The core losses are assumed to be negligible. It is shown that elongated cigar-shaped and flat dish-shaped cores can utilize effectively the magnetic properties of modern ferromagnetic materials.

INTRODUCTION

It is now well established that a core of suitable magnetic material increases the sensitivity of a receiving loop antenna (3). The benefit gained by employing a long coaxial core was discussed in some detail by Burgess (1).

A numerical discussion will be carried out in this paper for a solid spheroidal core coaxial with the loop. Curves will be plotted showing the dependence of the loop gain to the ratio of length to thickness of the core and the effective permeability of the core. The case of the axis of the loop perpendicular to the axis of symmetry of the spheroidal core will also be considered. Curves will also be plotted for this case. In both these problems it will prove convenient to employ prolate-spheroidal type coordinates.

All losses in the core are assumed to be negligible. This is justified at frequencies of the order of 200 kc. per sec. or less for ferromagnetic-ceramic materials (2).

CIRCULAR LOOP WITH SPHEROIDAL CORE

A prolate spheroid of magnetic permeability μ_1 is embedded in an infinite medium of permeability μ. The semimajor axis is b and the semiminor axis is a. A uniform magnetic field, whose component is $H_0 \exp(i\omega t)$ in the direction of the longitudinal axis, is applied to the spheroid. It will be assumed that the dimensions of the spheroid are much less than a wave length. The fields are then a solution of Laplace's equation.

A conventional cylindrical polar coordinate system (ρ,ϕ,z) is chosen with the origin at the center of the spheroid and the z axis coincident with the longitudinal axis of the spheroid. This is shown in Fig. 1. It is now convenient to introduce also prolate-spheroidal coordinates (4) whose family of spheroids are

$$[1] \qquad \frac{\rho^2}{c^2(\eta^2 - 1)} + \frac{z^2}{c^2\eta^2} = 1.$$

[1] *Manuscript received August 27, 1952.*
Contribution from the Radio Physics Laboratory, Defense Research Board, Ottawa, Canada.

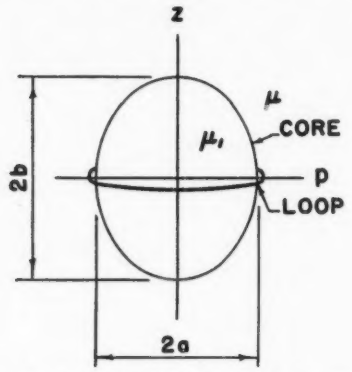

FIG. 1. Circular loop with spheroidal core of relative permeability μ_1/μ.

Associated with these are a family of hyperboloids which are

$$[2] \qquad \frac{\rho^2}{-c^2(1-\delta^2)} + \frac{z^2}{c^2\delta^2} = 1.$$

These coordinates (η,δ) shown in Fig. 2 are chosen to be confocal with the prolate spheroid in question. The constant c is such that

$$[3] \qquad \rho = c[(1-\delta^2)(\eta^2-1)]^{1/2}$$

and

$$[4] \qquad z = c\eta\delta.$$

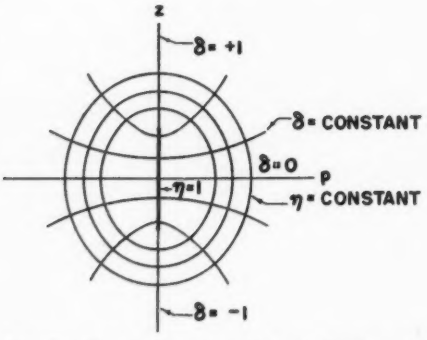

FIG. 2. The prolate-spheroidal coordinate system.

The metrical coefficients (4) are

$$[5] \qquad h_\delta = c\left[\frac{\eta^2-\delta^2}{1-\delta^2}\right]^{1/2}$$

$$h_\eta = c\left[\frac{\eta^2-\delta^2}{\eta^2-1}\right]^{1/2},$$

$$h_\phi = \rho.$$

Since in this problem symmetry about the longitudinal axis is evident it is only necessary to look for solutions of Laplace's equation that are independent of ϕ. The appropriate general solution is

$$[AP_n(\eta) + BQ_n(\eta)][CP_n(\delta) + DQ_n(\delta)]$$

where A, B, C, and D are constants and P_n and Q_n are Legendre functions of the first and second kind.

The resultant magnetic potential F outside the prolate spheroid can be written

$$F = P_1(\delta)cH_0[P_1(\eta) + BQ_1(\eta)] \tag{6}$$

since it must approach the value

$$F_0 = + c\eta\delta H_0 \tag{7}$$

at large values of η. The $Q_n(\delta)$ solutions have been rejected since the field is finite on the axis $\delta = \pm 1$.

The corresponding expression for the potential inside the spheroid is

$$F_1 = P_1(\delta)CP_1(\eta). \tag{8}$$

The boundary conditions are that the magnetic potential and normal flux density are continuous, i.e.,

$$\left.\begin{aligned} F_1 &= F \\ \mu_1 \frac{\partial F_1}{\partial \eta} &= \mu \frac{\partial F}{\partial \eta} \end{aligned}\right] \text{at } \eta = \eta_0. \tag{9}$$

The solution of these equations is carried out to give

$$B = \frac{(\mu_1 - \mu)P_1(\eta_0)}{\mu Q_1'(\eta_0)P_1(\eta_0) - \mu_1 Q_1(\eta_0)} \tag{10}$$

where the prime indicates a differentiation with respect of the argument of the function. In writing B in this form the identity $P_1'(\eta) = 1$ is used.

The voltage v induced in a circular loop of radius a contained in the plane $z = 0$ and encircling the prolate spheroid will now be calculated. This voltage is given by

$$v = -\frac{\partial M}{\partial t} = -i\omega M \tag{11}$$

where M is the total flux passing through the loop. But this flux M is also equal to the total flux passing into the upper half of the spheroid, that is

$$M = \int_0^1 2\pi\rho \frac{\mu}{h_\eta} \frac{\partial F}{\partial \eta} h_\delta \, d\delta \Bigg]_{\eta=\eta_0} \tag{12}$$

where the integral is to be evaluated over the surface $\eta = \eta_0$. Substituting in the values of ρ, h_δ, and h_η from equations [3] and [5] the expression for the induced voltage becomes after a simple integration:

$$v = v_0[1 + BQ_1'(\eta_0)] \tag{13}$$

where

$$v_0 = -i\mu\omega\pi a^2 H_0 N$$

and N is the number of turns of the loop.

The ratio v/v_0 is then the voltage gain of the antenna with the core relative to the same loop without the core. This ratio is plotted in Fig. 3 against b/a for various values of relative core permeability μ_1/μ. It can be seen that gains of the order of 25 are easily obtained, with the ratio of length to width of core of the order of six, for modern core materials that may have a relative permeability of the order of 200 or more.

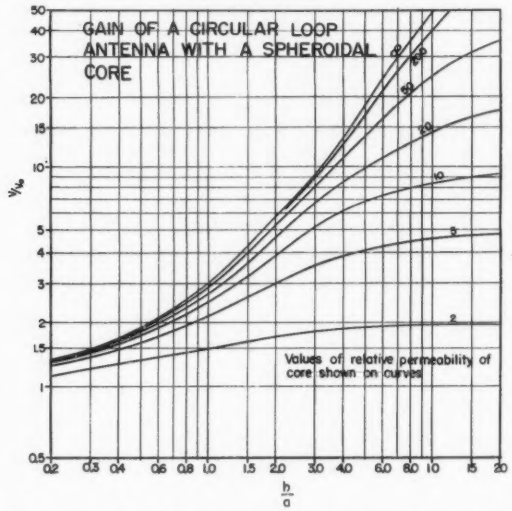

FIG. 3. The relative gain of a circular loop antenna of radius a with a solid spheroidal core of length $2b$.

The expression for the ratio v/v_0 has actually been generalized to include values of b/a less than unity. This means η_0 is imaginary and the coordinates actually transform over to oblate-spheroidal coordinates. This point will not be elaborated on since it can be readily verified that the same result is obtained if oblate-spheroidal coordinates were introduced at the outset.

ELLIPTICAL LOOP WITH SPHEROIDAL CORE

The other case of interest is when the loop is wound such that its axis is perpendicular to the axis of symmetry of the spheroid. The loop is then in the form of an ellipse and is oriented perpendicular to the loop shown in Fig. 1. The component H_0' of the magnetic field in the direction of the axis of the loop need only be considered. In this case the initial magnetic potential F_0' is given by

$$\begin{aligned} F_0' &= +H_0'\rho\cos\phi \\ &= +H_0'c(1-\delta^2)^{1/2}(\eta^2-1)^{1/2}\cos\phi \end{aligned} \qquad [14]$$

appropriate solutions are now

$$F' = \cos\phi\, P_1^1(\delta)\, H_0' c\, [P_1^1(\eta) + B' Q_1^1(\eta)] \quad [15]$$

and

$$F_1' = \cos\phi\, P_1^1(\delta)\, C'\, P_1^1(\eta) \quad [16]$$

where the superscript 1 signifies that the Legendre functions are of the associated type. The parameter η_0 is again allowed to be imaginary to include oblate-spheroidal solutions.

The same boundary conditions apply to this problem, namely that the potential and the normal flux are continuous at $\eta = \eta_0$. The constant B' can then be expressed in terms of known quantities and is found to be

$$B' = \frac{(\mu_1 - \mu) p p'}{\mu p q' - \mu_1 p' q} \quad [17]$$

where

$$p = P_1^1(\eta_0),\ p' = \frac{\partial p}{\partial \eta_0}$$

and

$$q = Q_1^1(\eta_0),\ q' = \frac{\partial q}{\partial \eta_0}.$$

The total flux M' threading the loop is now evaluated by integrating the normal flux density over half the area of the core, so that

$$M' = \int_{\delta=-1}^{+1} \int_{\phi=-\frac{\pi}{2}}^{+\frac{\pi}{2}} \frac{\mu}{h_\eta} \frac{\partial F}{\partial \eta}\, \rho h_3 d\phi d\delta \Big]_{\eta=\eta_0}. \quad [18]$$

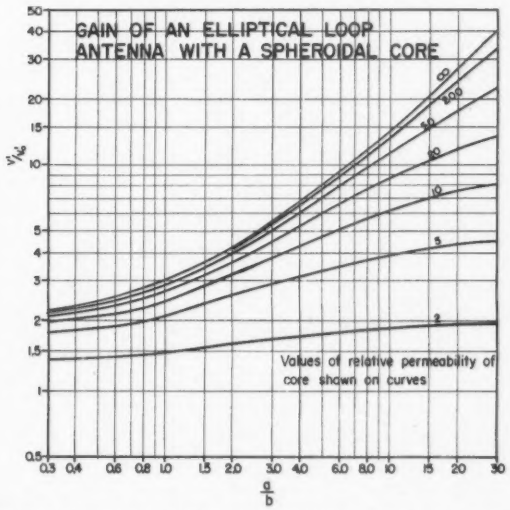

Fig. 4. The relative gain of an elliptical loop antenna with semiaxes a and b with a solid spheroidal core of radius a.

The expression for the induced voltage v' then becomes after integration

$$v' = v_0'(1 + B'q'/p') \qquad [19]$$

where

$$v_0' = -i\mu\omega\pi abH_0'N .$$

The ratio v'/v_0' is then the voltage gain of the antenna with the core relative to the same loop without the core. This ratio is plotted in Fig. 4 against values of the ratio a/b for values of relative core permeability μ_1/μ. High relative gains are also possible if the core is flat enough so that the ratio a/b is large. This type of flat dish-shaped core would seem to be a novel type that could have practical advantages over the more conventional cigar-shaped core.

ACKNOWLEDGMENT

This problem was suggested by Dr. T. W. Straker. The numerical calculations were carried out by Mr. D. V. Dickson.

REFERENCES

1. BURGESS, R. E. Wireless Engr. 23: 172-182. 1946.
2. GOLDSMITH, H. A. Product Eng. 20: 35–45. 1951.
3. POLYDOROFF, W. J. Radio-Electronic Eng. 46: 11–21. 1951.
4 STRATTON, J. A. Electromagnetic theory. McGraw-Hill Book Company, Inc., New York. 1941. p. 56.

THE INFLUENCE OF MANGANESE IN SOLID SOLUTION ON THE RECRYSTALLIZATION TEMPERATURE AND GRAIN SIZE OF PURE ALUMINUM SHEET[1]

By G. Marchand[2]

ABSTRACT

For sufficiently high rates of chill, manganese up to the limit investigated (2.5%) is retained in solid solution in cast α-aluminum. The general effect of manganese in solid solution is to raise the recrystallization temperature range of 83% cold-rolled sheet specimens but this increase is not monotonic. For instance, the temperature of complete recrystallization for a half-hour anneal is 400°C., 350°C., and 415°C. for 0.15%, 0.35%, and 1.4% manganese respectively. The primary recrystallized grain was coarser the higher the manganese content but the point of severe grain coarsening was shifted toward higher temperature so that, for sufficiently long annealing times, it is possible to obtain larger grain in low than in high manganese-bearing alloys. If part of the manganese is precipitated, the decrease in solute concentration results in a drop in the recrystallization temperature range and a decrease in grain size. In addition, the precipitated phase thus formed restricts grain growth and appears to refine the as-recrystallized grain, particularly in samples annealed with a high rate of heating.

INTRODUCTION

Manganese is one of the most common alloying additions used to improve the mechanical properties of aluminum. For this reason its effect on the recrystallization of aluminum alloys has attracted the attention of several investigators although the work done in this respect has often been of an incidental nature. It is well known that manganese, like any other metal addition, increases the recrystallization temperature range* of pure aluminum. For example, Kratz (11) found that whereas pure aluminum (99.997%) cold-rolled 90% recrystallized at 220°C. for a two-hour annealing period, an addition of 0.1% manganese increased this temperature to 350°C. for the same annealing time and amount of deformation. Phillips (16), quoting the results from some unpublished work by Spillett, states that additions of 1% Mn to 99.92% purity aluminum increased the recrystallization temperature by about 60°C. Phillips adds that, up to 0.25%, manganese has little influence on the grain size of rolled aluminum, but above this limit it promotes coarsening and nonuniformity of grain size. Bungardt and Osswald (4) investigated the effect of manganese additions on the recrystallization temperature range of several aluminum alloys and always found them to raise this temperature range. They determined in particular the temperatures of initial and complete recrystallization of aluminum–manganese alloys with impurity contents ranging between 0.04% and 0.32%. For a cold reduction of 80-85% and a 30-min. anneal both the temperatures of initial and of complete recrystallization were increased by manganese additions up to 0.15%. From

[1] *Manuscript received June 18, 1952.*
Contribution from Aluminium Laboratories Limited, Kingston, Ont.
[2] *Metallurgist, Physics and Physical Metallurgy Divisions.*

**The recrystallization temperature range is understood here as the interval of temperature in which recrystallization begins and ends for a fixed annealing time.*

0.15% to 1.4% manganese, while the temperature of initial recrystallization increased linearly from 330°C. to 375°C., the temperature of complete recrystallization remained constant at 400°C.

Although the present investigation is not concerned primarily with grain growth, the work of Beck (1) on binary aluminum–manganese alloys warrants attention. He showed that manganese present as a second phase in an aluminum matrix had a very strong restrictive influence on grain growth, re-solution of this phase during annealing at high temperatures creating conditions favorable for secondary recrystallization. This observation has been supported by Lacombe (12) who found that the rate of solution of the second phase determined whether or not secondary recrystallization would take place. These papers certainly emphasize the importance of defining the metallographic state of the material on which recrystallization studies are to be made.

This point, not always made clear in previous investigations, appeared particularly important in the case of aluminum–manganese alloys in which, as will be seen subsequently, metastable conditions are likely to exist. It thus appeared worth verifying the results of previous investigations in a fairly systematic way. As a first step it was planned to study in some detail the effect that manganese in solid solution, and as a precipitate, could have on the recrystallization temperature range and grain size of rolled aluminum sheet; a brief correlation would also be made with alloys of commercial purity.

THE ALUMINUM END OF THE ALUMINUM–MANGANESE EQUILIBRIUM DIAGRAM

Examination of the aluminum end of the aluminum–manganese diagram (see Fig. 1) should prove useful in the subsequent discussion. The solid solubility of manganese in aluminum with less than 0.01% Fe was determined by Dix, Fink, and Willey (6) to be 1.82% at the eutectic temperature, whereas Butchers and Hume-Rothery (5) working later on with materials of similar purity reported 1.35%. Brief checks made on the solubility limit during the present investigation favored the values obtained by the first investigators. Until recently it has been supposed that the equilibrium phase separating out in these alloys corresponds to the composition $MnAl_6$. Hume-Rothery (14) and his co-workers, however, have shown that besides $MnAl_6$ a metastable phase may precipitate from the supersaturated solid solution at temperatures lower than about 600°C. This phase, termed "G", has the approximate formula $MnAl_{12}$ and it transforms eventually into the equilibrium phase $MnAl_6$. The presence of as little as 0.2% of iron or silicon prevents its formation altogether (13).

Iron drastically reduces the solubility of manganese in aluminum, from 1.82% in super purity aluminum down to 0.65% for that containing about 0.05% iron, as reported by Dix and Keith (7).

The equilibrium diagram presents a eutectic point at 1.95% manganese. Under conditions created by chill-casting, this eutectic horizontal is shifted, but while shifting it displays a strange behavior for, instead of moving towards lower alloying contents, it appears to be pushed in the opposite direction. This results in

the disappearance of the eutectic with increasing degree of chill. This fact has led some investigators (7) to believe that the eutectic, because it is not visible under the light microscope, must be present as a submicroscopic dispersion which they have called a "dispersoid". Later, Hofman (9) showed by lattice parameter measurements that in rapidly cooled aluminum–manganese alloys, the manganese remained in solid solution even up to 4%, which is far beyond the eutectic point.

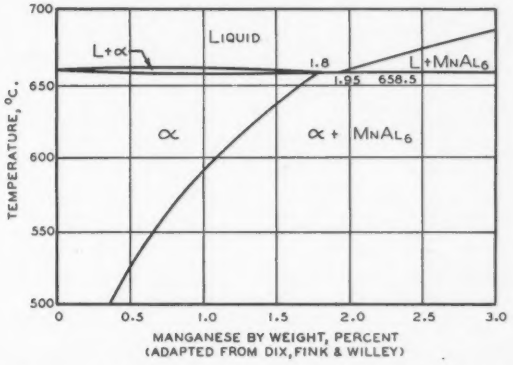

FIG. 1. Aluminum end of the aluminum–manganese equilibrium diagram.

In the present work this unusual phenomenon was also checked by measuring the lattice parameter of a series of high purity binary alloys by the X-ray back reflection method. The results are presented in Fig. 2. Up to 1.5% the measurements were made on alloys homogenized in the α-field and on chill-cast alloys above that composition. A straight line may be drawn through this set of points extending even beyond the eutectic composition. The agreement with Hofman's results is reasonably good and we may safely conclude that the manganese, which we were unable to see under the light microscope or the electron microscope, is not present as a second phase but is in solid solution.

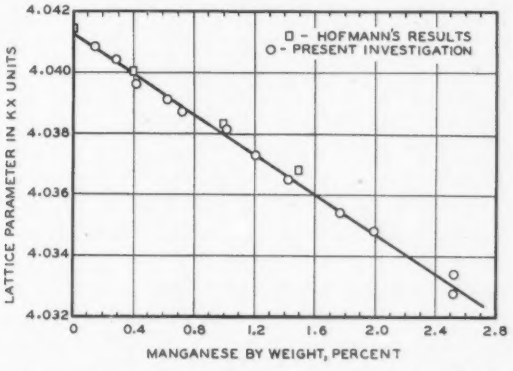

FIG. 2. Variation of lattice parameter with amount of manganese in solid solution in aluminum.

EXPERIMENTAL MATERIALS AND PROCEDURE

A series of 11 binary aluminum–manganese alloys were prepared, the analyses of which are given in Table I.

The purity of the base metal was given by the supplier as being 99.994%, the impurities being 0.0015% iron, 0.0015% copper, 0.0025% silicon. The manganese was added by means of a hardener which was obtained by reducing manganese chloride in the base metal. All the alloys were melted in an alundum crucible and graphite tools were used to avoid contamination. The melts were heated up to

TABLE I

MANGANESE CONTENT OF ALLOYS INVESTIGATED

Alloy No.	Mn content, % by weight
1	0.15
2	0.29
3	0.42
4	0.63
5	0.73
6	1.02
7	1.21
8	1.43
9	1.77
10	1.99
11	2.52

720-750°C., stirred, fluxed with chlorine for one minute, and then cast in a graphite mold which was heated to about 450°C. to ensure a good ingot surface. The size of the ingots for alloys No. 1 to No. 8 was 1 in. × 1 in. × 6 in., and for the remaining three alloys small plates 1/4 in. thick were cast in a cold iron mold. The cast ingots were used for micrographic examination and for the lattice parameter measurements already described.

Alloys 1 to 8, those that could be easily obtained as solid solution under equilibrium conditions, were used for recrystallization studies. The cast ingots were cold-rolled down to 0.300 in., homogenized between 640°C. and 650°C. and cold-rolled again down to a nominal thickness of 0.050 in., i.e. 83% cold reduction. This sheet was cut into 1 in. wide samples which were annealed for 30-min. in a salt bath at temperatures ranging from 225 to 550°C. The progress of recrystallization was followed by hardness measurements, microscopic examination, and by X-ray back reflection patterns. For microscopic examination the surface was etched either electrolytically or in the acid mixture (HCl–HF–HNO_3). Grain size measurements were made at such a magnification as to produce an average grain image of approximately the same size for all samples. Arbitrarily, the diameter at right angles to the rolling direction* of 75-150 grains, picked up at regular intervals all over the surface of the specimens, was measured and the arithmetical average of these readings was taken as the average grain size. Com-

*The grain size was on the average sufficiently equiaxed to warrant this simplification.

parative measurements were also carried out on some samples by the intercept method. The average grain size determined this way was about 0.6 times that found with the first method. This first procedure allows one to cover relatively large areas with a minimum of effort and also it yields results which lend themselves to spatial grain size analysis. Grain size measurements, usually carried out on the rolled surface of the specimens either electrolytically or chemically etched, were also repeated on several samples ground to approximately half their original thickness in order to make a comparison between surface and subsurface grains.

RESULTS

The results from the hardness measurements on alloys cold-rolled 83% and annealed 30 min. in a salt bath are presented in Fig. 3. A definite shift of the softening curves towards the higher temperatures may be observed as the concentration of the manganese increases. The slopes of the middle portion of the curves also increase when going to the right; in other words, for this fixed annealing time, the softening process occurred within a narrower temperature range at

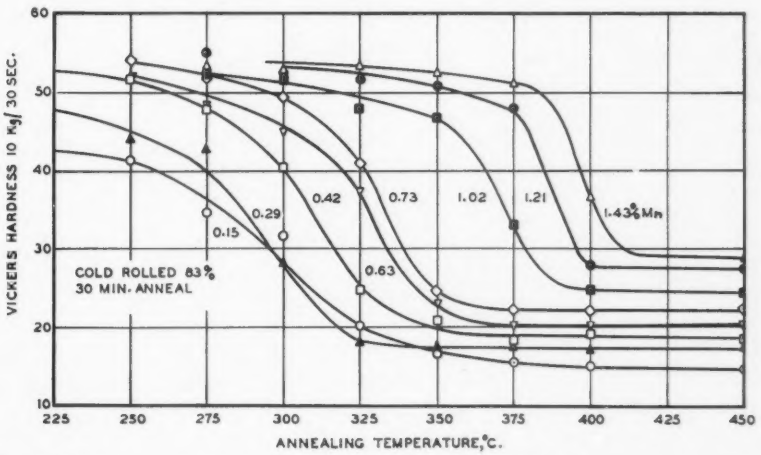

FIG. 3. Softening curves of single phase aluminum-manganese alloys annealed at various temperatures.

higher manganese contents. This feature results in the 0.15% manganese curve crossing the 0.29% curve.

From this diagram the end point of recrystallization was estimated and replotted in Fig. 4 against the manganese content of the alloys. In the same figure, an attempt has been made to represent the combined results of visual and X-ray examination of the specimen surfaces. The latter method has been used to locate the curve giving the temperature of initial recrystallization. It is not possible to determine the temperature of initial recrystallization from the hardness curves because they do not display a characteristic change at that point. On a macroscale the phenomenon of recovery blends into that of recrystallization.

A peculiarity of the upper curve is that it presents a maximum in the vicinity of 0.15% manganese followed by a minimum at about 0.35%. Similar characteristics have been found by other investigators on aluminum–magnesium alloys (2, 15), and aluminum–copper alloys (3) but were not observed by Bungardt and Osswald (4) in aluminum–manganese alloys. The latter workers, however, ap-

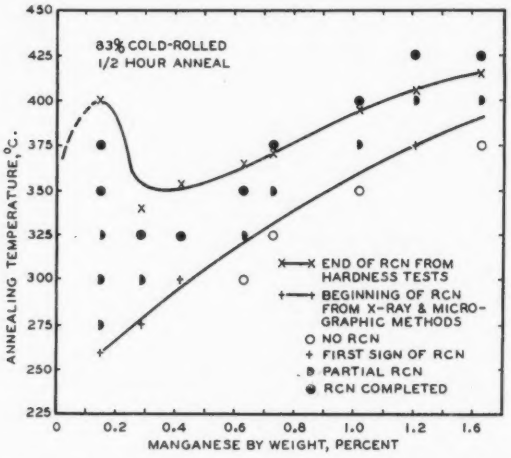

FIG. 4. Recrystallization temperature range of aluminum in function of the manganese content of the solid solution.

parently did not make their measurements on solid solution types of alloys so that their results are not strictly comparable to the present ones. In the case of aluminum–magnesium alloys a definite maximum in the recrystallization temperature curves was observed at 1.5% and a minimum at about 4.5% magnesium. It has been suggested (15) that the temperature drop following the maximum was due to the increased strain hardening resulting from magnesium additions and that the temperature rise beyond 4.5% was the result of precipitation of beta phase occurring during annealing thus delaying recrystallization. If one accepts this explanation for the recrystallization temperature drop then the initial temperature rise (from zero to 0.15% manganese or from zero to 1.5% magnesium) is difficult to explain for the strain hardening increases continuously with the amount of alloying elements. Although the explanation for the second temperature rise based on precipitation is plausible it does not fit the present observations because recrystallization was found to occur before any great amount of precipitation took place. It is suspected that these characteristics are related to the type of deformation used to introduce cold work in the metal.

One will notice in Fig. 4 a discrepancy, especially at low manganese contents, between the end point of recrystallization as estimated from the hardness tests and that determined by X-ray and microscopic methods. Further microscopic examination of the samples showed that recrystallization started earlier and was

completed earlier at the surface of the samples than in the subsurface layers. Owing to the fact that the hardness indenter penetrates some distance below the surface, the hardness figure obtained will be representative of both the surface and subsurface layers. This together with the above-mentioned observations explains the discrepancy between the results obtained by the different techniques.

The effect of a precipitation treatment of 24 hr. at 570°C. on the softening curve of the 1.21% Mn alloy is shown in Fig. 5. For purposes of comparison annealing curves for the single-phase 1.21% and 1.02% Mn alloys are also shown.

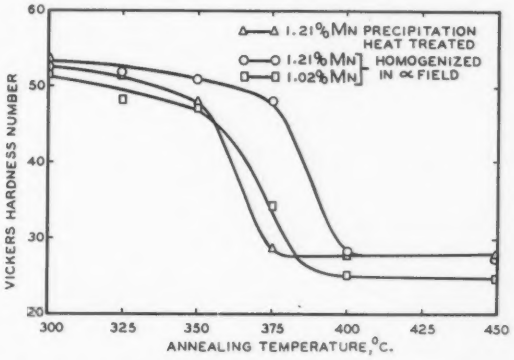

FIG. 5. Effect of a precipitation treatment at 570°C. on the annealing curve of a binary aluminum-manganese alloy.

The precipitation treatment has produced a pronounced decrease in the recrystallization temperature range, presumably owing to a lowering of the concentration of manganese in solid solution. It can be seen here that the temperature of complete recrystallization for precipitated material is 380°C. which, from Fig. 4, corresponds to the temperature of complete recrystallization for an alloy containing either 0.05%, 0.25%, or 0.8% manganese in solid solution. On the other hand, the solubility of manganese at 570°C. is 0.8% suggesting that this latter value was the one which determined the recrystallization temperature range of the precipitated alloy.

The initial grain size of the 0.300 in. thick plates after the homogenization treatment at 645°C. and prior to the 83% cold reduction ranged from 1 to 5 mm., the finest grain being observed at higher manganese concentrations. The grain size in this case was determined by the rate of grain growth.

The trend toward finer grain with higher manganese was generally reversed on the as-recrystallized samples as can be seen in Fig. 6 in which the results of grain size measurements on some of the alloys, cold-rolled 83% and annealed a half-hour in a salt bath, have been plotted against the annealing temperature. For any given alloy, as the annealing temperature increases, the grain size decreases to a point where a minimum is reached. This minimum is located at a higher temperature the higher the manganese content. For the 0.42%, 0.73%,

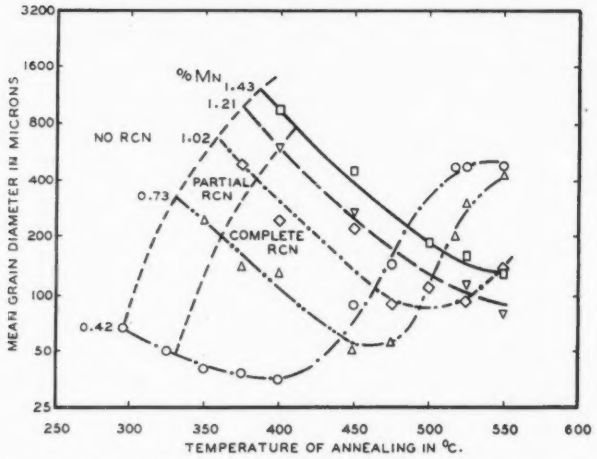

FIG. 6. Grain size of single phase aluminum-manganese alloys after annealing 30 min. at indicated temperatures.

and 1.02% manganese alloys the increase in grain size following this minimum is due to grain growth. It appears that the grain size curves for the 1.21% and 1.42% Mn alloys have not reached their minimum at 550°C. (the maximum temperature at which the salt bath could be operated safely). It was observed microscopically, in these cases, that a small amount of precipitation had taken place for annealing temperatures in excess of 450°C. This precipitation would favor a refinement of the grain which explains why the minimum in the grain size curves for these alloys is lower than would be expected if they remained single-phased.

Fig. 7 shows grain size curves of alloys containing 0.15%, 0.29%, and 0.42% manganese. In this instance, however, measurements were made on samples abraded approximately halfway through their thickness. The surface grain size curve for the third alloy (0.42% Mn, bottom curve) is included in order to relate the results of these measurements with those given previously. Within the limits of experimental error, there does not appear to be too great a difference between the three alloys. It is clear that at the lower annealing temperatures the grains in the subsurface layers are much coarser than those at the surface and the same observation was made even when the samples were ground before annealing so that this effect is not due to some external factor such as a higher heating rate at the surface than in the center of the samples. A microhardness survey across the thickness of a cold-rolled sample containing 0.42% Mn showed that the surface layers were about 30% harder than the center ones suggesting that a higher degree of strain hardening may be responsible for the finer surface grain. Because of grain growth this difference decreases as the annealing temperature increases. It should be added that this difference between surface and subsurface grain size was generally less in coarse-grained samples.

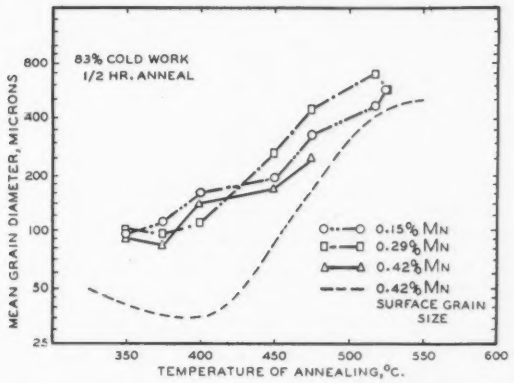

FIG. 7. Inner grain size of single phase aluminum-manganese alloys annealed at various temperatures.

The results given up to now were all obtained on specimens annealed in a salt bath, which gives a rapid rate of heating. In Fig. 8 the grain size versus manganese content has been plotted for a slower rate of heating. These samples were put in a cold furnace and brought up to 450°C. in half an hour then held 10 min. at temperature. As would be expected from the previous results, above 0.40% Mn content the grain size generally increased with the amount of alloying element

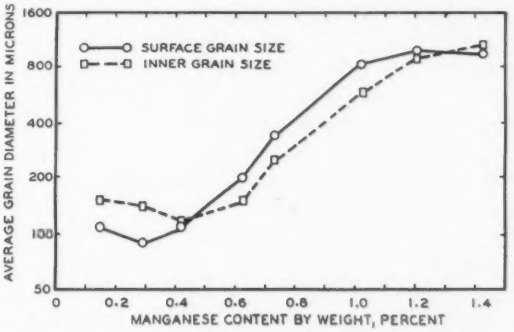

FIG. 8. Grain size of aluminum-manganese binary alloys annealed 10 min. at 450°C. with an average heating rate of 14°C. per min.

in solution. It is possible that the slight dip in the curves from 0.15% to 0.40% has some significance, because the base metal without manganese additions, cold-rolled 75% and annealed under the same conditions, had a grain size between 300 and 400 μ. Hence it appears that the first manganese additions either have a grain refining effect or perhaps only restrict grain growth. It will also be noticed that the percentage difference between surface and subsurface grain sizes is not as great as in the previous diagram.

Specimens of the 1.21% manganese alloy given the precipitation treatment described before, i.e. 24 hr. at 570°C. were annealed at 450°C. with a slow rate of heating (i.e., 30 min. to reach 450°C.). The grain sizes of the surface and subsurface were found to be 215 and 260 μ respectively. On Fig. 8 this grain size corresponds to that obtained with approximately 0.7% manganese in solid solution. Now it will be recalled that the solid solubility of manganese in aluminum at 570°C. is 0.80% so that it appears that with slow rates of heating the grain size is almost entirely defined by the manganese in solid solution and not so much by the precipitate. With rapid rates of heating the position is very different. For example, taking the 1.21% manganese alloy annealed in a salt bath at 450°C. the grain size obtained with all the manganese in solid solution was 270 μ as compared with 26 μ for precipitated material. If the refining action of the precipitate is expressed as the ratio of the grain size in the single phase condition to that in the precipitated condition the following ratios for the two heating rates are obtained.

Slow heating rate (450°C.) 880: 215 $\sim$ 4:1
High heating rate (450°C.) 270: 26 $\sim$ 10:1

The grain refining action of the precipitate is probably due to an alteration in the ratio of rate of nucleation to rate of grain growth. We know the manganese precipitate restricts growth; it is not improbable that it also favors nucleation by increasing the number of zones of greater disturbance, and thereby the number of potential nuclei in the cold-worked structure. A slow rate of heating may render these zones inoperative by allowing them to recover down to the energy level of the mass of the metal.

We now have to consider the effect of heating rate on the grain size of homogeneous alloys. Eastwood *et al.* (8) made an extensive study of this factor on the grain size of several aluminum alloys. One of their conclusions was that the annealed crystal size of single-phase alloys was independent of the heating rate. This was questioned in the discussion of the paper on the basis that grain growth had certainly occurred in certain, and possibly in all, cases. The present data do not support Eastwood's views. On all alloys on which detailed measurements were made, the lower rate of heating to 450°C. gave a much larger grain size than a high heating rate to the same temperature. Actually this would be expected from the type of curves found in Fig. 6. An alloy in which the grain size decreases with increasing annealing temperature would certainly be expected to have a large grain when brought up slowly to a given temperature since recrystallization would very likely have started, during the heating process, at a lower temperature. In the present case, an interesting correlation is found between the grain size given by the slower anneal and that which would be given by extrapolating the curves of Fig. 6 to the temperature of initial recrystallization determined from the lower curve of Fig. 5. The results are shown in Table II.

The agreement between the columns 1 and 2 of Table II is possibly more than a mere coincidence, and, if so, would indicate that about the same number of nuclei formed in the half-hour that the samples took to reach 450°C. as would form during heating half an hour at the nucleation temperature. Further work along this line might lead to some interesting generalizations.

TABLE II

GRAIN SIZE VARIATION WITH DIFFERENT CONDITIONS OF ANNEALING

% Mn	Grain size in microns		
	Slow heating up to 450°C.	Extrapol. to nucleation temp., 30-min. anneal	Fast heating, 30 min. at 450°C.
1.43	940	1200	400
1.21	960	950	240
1.02	820	750	140
0.73	340	320	55
0.42	110*	65	75*

**A certain amount of grain growth may have taken place in these samples.*

As a practical note it may be interesting to point out that the minimum in the grain size vs. manganese content curve (see Fig. 8) obtained under conditions not unlike those of an industrial anneal, corresponds also to a minimum in the recrystallization temperature (Fig. 4). Thus because of the small grain size and low annealing temperature it is desirable to keep the level of manganese in solid solution down to 0.30% to 0.40% which is in fair agreement with Phillips (16) observations. Of course this rule is valid only in so far as the commercial alloys behave like the pure binary alloys considered so far. This was verified in our Laboratories by another investigator (10) whose results will be briefly summarized.

Starting with a base metal containing 0.38% iron, 0.25% silicon, besides traces of the impurities usually found in commercial grade aluminum, seven alloys were prepared and chill-cast in a small graphite mold. The lattice parameter, Vickers hardness, and electrical conductivity of these alloys were measured in the as-cast conditions and the results are shown in Figs. 9*a*, 9*b*, and 9*c*. The lattice parameter and hardness results are furthermore related to those obtained for the high purity alloys. The near parallelism of these first two sets of curves at low manganese contents indicates that the degree of solution of the manganese in the matrix is nearly the same whatever the purity of the base metal. The smoothness of the curves of the commercial base alloys also indicates that supersaturation takes place over the whole range investigated although the amount of dissolved manganese is less as the total concentration of manganese increases. For instance at 1.39% manganese, about 1.16% is in solid solution in the matrix and the remaining 0.33% is associated with the α(Al–Fe–Si)-constituents. In fact a noticeable increase in the size of the eutectic "script" with manganese additions may be observed. Fig. 10 represents the "script" in an alloy containing 0.4% iron and 0.2% silicon, whereas Fig. 11 shows the same alloy with 1.25% manganese. The effect of a precipitation heat treatment at 525°C. and of a re-solution treatment at 635°C. was investigated on an alloy containing 1.25% manganese, 0.41% iron, 0.30% silicon, 0.02% copper. The variation of the conductivity, lattice parameter, and hardness is given in Table III.

The conductivity and lattice parameter have increased and the hardness decreased after 66 hr. at 525°C. Neglecting the effect of small differences in impurity

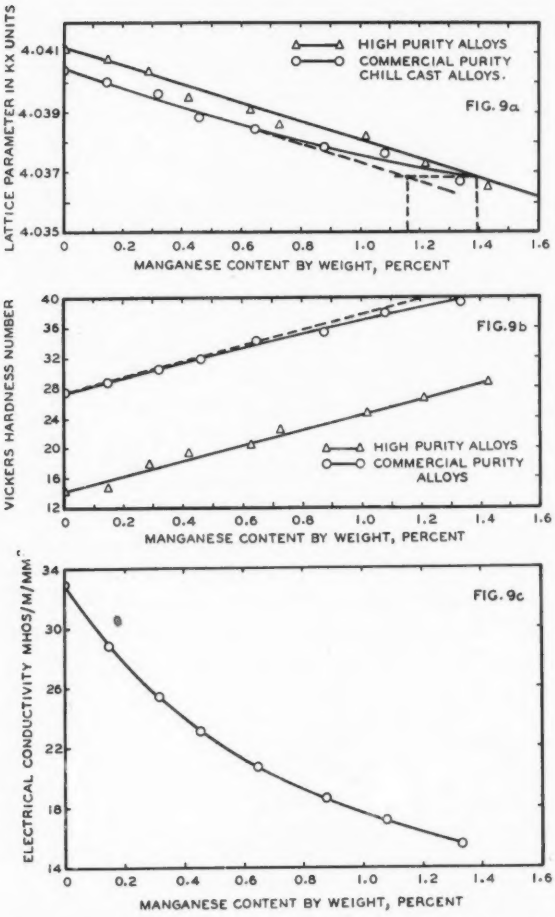

FIG. 9*a*. Lattice parameter variation with manganese content in Al–Mn alloys.
FIG. 9*b*. Variation of hardness values with manganese content in Al–Mn alloys.
FIG. 9*c*. Variation of the electrical conductivity of commercial grade aluminum with manganese additions.

TABLE III

INFLUENCE OF THERMAL HISTORY ON SOME PHYSICAL PROPERTIES OF A COMMERCIAL GRADE ALLOY CONTAINING 1.25% MANGANESE

Treatment	Conductivity, mhos/m./mm.²	Lattice constant, kX units	Hardness, V-10/30
A, chill-cast	16.2	4.0370	40.2
B, A, 66 hr. at 525°C.	25.0	4.0398	33.5
C, B, 16 hr. at 635°C.	19.8	4.0386	—

PLATE I

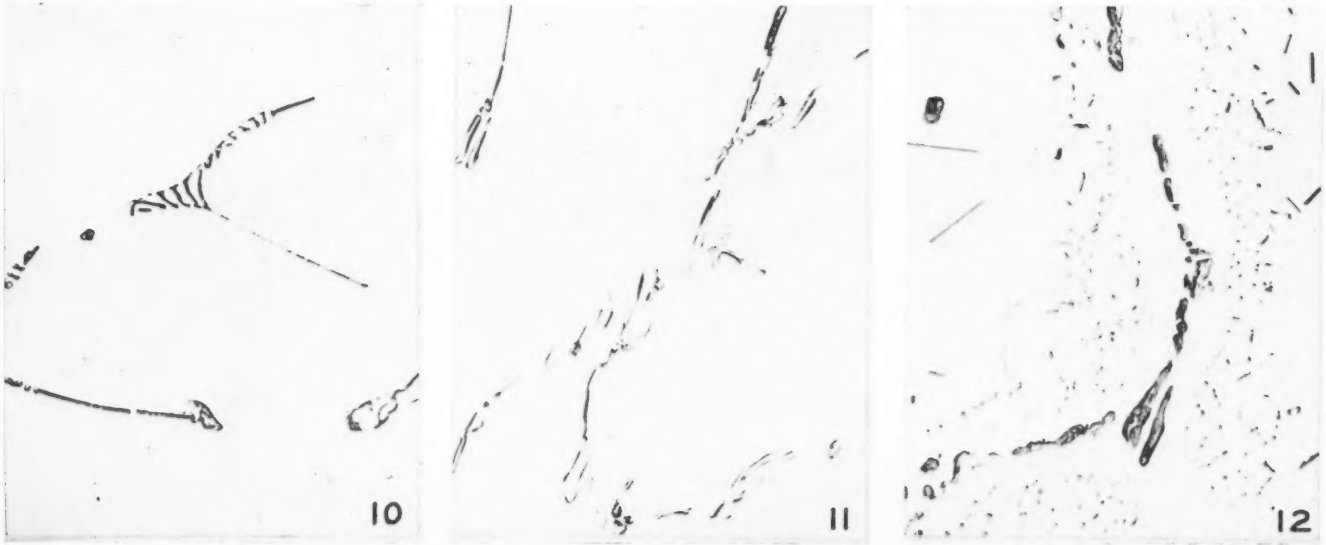

FIG. 10. 0.4% Fe, 0.2% Si, remainder aluminum, chill-cast, as electrolytically polished. ×500.

FIG. 11. 0.4% Fe, 0.2% Si, 1.25% Mn, remainder aluminum, chill-cast, as electrolytically polished. ×500.

FIG. 12. 0.4% Fe, 0.3% Si, 1.25% Mn, remainder aluminum, chill-cast, and heated 66 hr. at 525°C. ×500.

content, the residual concentration of manganese in solid solution after heat treatment at 525°C. can be estimated from the curves of Fig. 9 to be about 0.35% which corresponds to the manganese content necessary to obtain the minimum grain size and recrystallization temperature for binary alloys. The extent of precipitation after this treatment may be seen from a comparison of Figs. 11 and 12.

As would be expected a re-solution treatment of 16 hr. at 635°C., only 20°C. below the eutectic temperature, did not restore the original as-cast properties since the equilibrium solubility at that temperature is less than the actual amount of manganese retained in solution by chill casting. The values obtained (Item C in Table III) when compared with the curves of Fig. 9 give a solubility of 0.66% at 635°C., an acceptable approximation of the values given by Dix and Keith (7) (0.65% at the eutectic temperature with about 0.05% iron). In consistence with the above facts, it is known from practical experience that a chill-cast commercial purity alloy containing, say, 1.25% manganese has a relatively high recrystallization temperature and a large grain size when fabricated without thermal treatment. If a precipitation treatment is carried out prior to hot-rolling, this alloy is much easier to roll and the final product recrystallizes at lower temperatures with an even grain size which can be held within the limits of commercial tolerances.

CONCLUSIONS

It has been verified by lattice parameter measurements that in aluminum–manganese alloys solidified with a sufficiently high degree of chill, most, or all, of the manganese remains in solution. In these chill-cast structures, the course of recrystallization is thus largely determined by the amount of manganese in solid solution.

The temperature at which recrystallization is complete was determined by hardness measurements on a range of high purity alloys containing up to 1.42% manganese in solid solution. For 83% cold-rolled sheet annealed half an hour in a salt bath, the temperature of complete recrystallization was found to be 400°C. at 0.15% manganese, decreasing to 350°C. at 0.35% and then rising again to 415°C. at 1.42% manganese. The temperature of initial recrystallization determined by X-ray and micrographic methods showed a continuous increase from 260°C. at 0.15% to 390°C. at 1.42% manganese.

The grain size in the single-phase alloys and in the absence of grain growth is finer the higher the annealing temperature. This temperature effect is, however, less pronounced at low manganese contents. On the other hand increasing concentration of the manganese in solid solution retards grain growth. The grain size in these alloys is finer the higher the rate of heating and it is suggested that this effect is related to the temperature dependence of the grain size.

Precipitation of part of the manganese, besides preventing grain growth, has a strong refining action on the as-recrystallized grain size. This refinement, however, appears to be a function of the heating rate, being greater with a high rate of heating.

ACKNOWLEDGMENT

The author wishes to thank Mr. E. C. W. Perryman for his helpful discussion of this paper.

REFERENCES

1. BECK, P. A., HOLSWORTH, M. L., and SPERRY, P. R. Trans. Am. Inst. Mining Met. Engrs. 180: 163-192. 1949.
2. BUNGARDT, W. and OSSWALD, E. Z. Metallkunde. 30: 202-205. 1938.
3. BUNGARDT, W. and OSSWALD, E. Z. Metallkunde. 31: 45-55. 1939.
4. BUNGARDT, W. and OSSWALD, E. Z. Metallkunde. 32: 368-375. 1940.
5. BUTCHERS, E. and HUME-ROTHERY, W. J. Inst. Metals, 71: 87-91. 1945.
6. DIX, E. H., FINK, W. L., and WILLEY, L. A. Trans. Am. Inst. Mining Met. Engrs. 104: 335-352. 1933.
7. DIX, E. H. and KEITH, W. D. Trans. Am. Inst. Mining Met. Engrs., Inst. Metals Div. 315-333. 1927.
8. EASTWOOD, L. W., JAMES, R. W., and BELL, M. F. Trans. Am. Inst. Mining Met. Engrs. 133: 124-136. 1939.
9. HOFMAN, W. Aluminium, 20: 865-872. 1938.
10. HOWE, R. M. Aluminium Laboratories Limited: Kingston. Unpublished work.
11. KRATZ, E. Aluminium-Arch. 6: 1-25. 1937.
12. LACOMBE, P. Métaux, corrosions-inds. 26: 392-409. 1951.
13. LITTLE, K. and HUME-ROTHERY, W. J. Inst. Metals, 74: 521-524. 1948.
14. LITTLE, K., RAYNOR, G. V., and HUME-ROTHERY, W. J. Inst. Metals, 73: 83-90. 1947.
15. MICHAUD, R. and SEGOL, E. Compt. rend. 204: 980-983. 1937.
16. PHILLIPS, H. W. L. J. Inst. Metals, 68: 47-105. 1942.

MAP PROJECTIONS FOR POLAR LATITUDES[1]

By Warren L. Godson[2]

ABSTRACT

The general properties and defining relations of the Lambert conformal conic projection, and its limiting case the Polar Stereographic projection, are examined in relation to requirements for aeronautical and meteorological purposes in polar regions. In particular, the Polar Stereographic projection is compared to the Ney modified Lambert projection. Criteria for minimum mean absolute scale error and for zero algebraic mean scale error are derived for the former projection, and it is shown that a Polar Stereographic projection with minimum mean scale error is the most suitable polar projection available if conformality is a major requirement.

1. INTRODUCTION

For purposes of both meteorology and air navigation, a conformal map projection, preserving angles, is desirable. If transpolar navigation or meteorological charts are required, this effectively limits consideration to the polar stereographic projection, when the essential simplicity of this projection (straight meridians, concentrically-circular parallels of latitude) is taken into account. Recently an alternative has been suggested, namely the Ney (3) modified Lambert conformal conic projection.

By sacrificing rigid conformality (maximum relative error less than 0.3%), Ney claims a significant reduction in the magnitude of scale errors for a mapping from 65 to 90°N. Since the polar stereographic projection is merely a limiting case of a Lambert conformal conic, the above statement does not appear plausible. It will, in fact, be shown in this paper that the sacrifice of conformality (no matter to what small degree) is entirely unnecessary. Similar conclusions have been reached independently by R. D. Hutchison (unpublished) and by Mack and Sharp (2).

2. LAMBERT CONFORMAL CONIC AND POLAR STEREOGRAPHIC PROJECTIONS

The basic theory of conformal and other conic projections has been given by Adams (1) and need not be reproduced here. In fact, only two equations defining the construction and properties of a Lambert conformal conic will be required, namely:

$$[1] \qquad R_\phi = K\left(\frac{\cos\phi}{1+\sin\phi}\right)^L\left(\frac{1+e\sin\phi}{1-e\sin\phi}\right)^{Le/2}$$

$$[2] \qquad m_\phi = \frac{R_\phi L}{a\cos\phi}(1-e^2\sin^2\phi)^{\frac{1}{2}}.$$

In thsee relations, R_ϕ denotes the map radius of a latitude line, K denotes a constant, ϕ denotes the geodetic latitude, L denotes the cone constant (ratio of angle between meridians on the map to the angle between the same meridians

[1] *Manuscript received October 16, 1952.*
Contribution from the Meteorological Division, Department of Transport, Canada. Published by permission of the Controller of Meteorological Services.
[2] *Research Section, Meteorological Division, 315 Bloor St. West, Toronto 5, Ontario.*

on the earth), e denotes the earth's ellipticity, m_ϕ denotes the map magnification at any latitude (ratio of map distance to earth distance, independent of direction for a conformal projection), and a denotes the earth's equatorial radius. For simplicity, it will be assumed that the actual standard map scale (e.g., 30 nautical miles per inch) is taken care of separately.

The normal conic projection has two standard latitudes, ϕ_1 and ϕ_2, say, at which m_ϕ has the value of unity. Between these two latitudes, $m_\phi < 1$; beyond these latitudes $m_\phi > 1$. At the north pole, since $L < 1$, m_ϕ is infinitely large, as can be seen from a combination of [1] and [2] giving

$$[3] \qquad m_\phi = \frac{KL}{a \cos \phi}\left(\frac{\cos \phi}{1 + \sin \phi}\right)^L\left(\frac{1 + e \sin \phi}{1 - e \sin \phi}\right)^{Le/2}(1 - e^2\sin^2\phi)^{\frac{1}{2}}.$$

In general, K and L can be so chosen that: $m_{\phi_1} = m_{\phi_2} = 1$. Consider now the case when the northern standard parallel, ϕ_1, is moved northward to the pole. If $\phi_1 = \pi/2$, m_{ϕ_1} can be finite only if L = 1, so that a fixed or standard map scale can be achieved at only a single latitude, denoted by ϕ_0 in what follows. Since $L = 1$, the conic now represents a circumpolar projection and is the Polar Stereographic projection. It can simply be seen from [3] that m_ϕ has a minimum value at the pole when $L = 1$, and varies monotonically with latitude.

If the northern standard parallel, ϕ_1, is chosen as very near the pole, computations show that L must be only slightly less than unity. Ney (3) suggested a modification of the Lambert projection, with ϕ_1 very near the pole, in which latitude lines were evaluated from [1] using the true value of L, but in which longitude lines were plotted as if L were unity, giving a polar projection. In such a case, the north–south magnification is m_ϕ, as defined by [2], but the east–west magnification is m_ϕ/L, so that the resulting projection is no longer strictly conformal. Ney argued that this projection would have smaller scale errors than the Polar Stereographic projection since the latter has a minimum magnification at the pole, whereas the magnification in the former case returns to unity at ϕ_1. However, it can be shown from [3] that if ϕ_1 is very near the pole, the latitude of minimum m_ϕ will also be very near the pole. This can also be deduced intuitively from the fact that m_ϕ at ϕ_1 is unity, whereas m_ϕ at the pole is infinite. In the next two sections, mean scale errors on these two projections will be evaluated and compared.

3. CHOICE OF BEST POLAR STEREOGRAPHIC PROJECTION

The equations for a polar stereographic projection can be obtained from those for a Lambert, [1] and [2], by setting L equal to unity. Thus

$$[4] \qquad R_\phi = \frac{K \cos \phi}{1 + \sin \phi}\left(\frac{1 + e \sin \phi}{1 - e \sin \phi}\right)^{e/2}$$

$$[5] \qquad m_\phi = \frac{K(1 - e^2\sin^2\phi)^{\frac{1}{2}}}{a(1 + \sin \phi)}\left(\frac{1 + e \sin \phi}{1 - e \sin \phi}\right)^{e/2}.$$

At the single standard latitude, ϕ_0, m_ϕ has the value of unity. The relative scale error at any latitude, σ_ϕ, is thus given as

$$[6] \qquad \sigma_\phi = m_\phi - 1.$$

Since sin ϕ varies only slowly with latitude in the polar regions, the small terms due to eccentricity may be considered virtually constant. Thus, to a high degree of approximation, from [5] and [6],

$$\sigma_\phi = \frac{\sin \phi_0 - \sin \phi}{1 + \sin \phi}. \tag{7}$$

ϕ_0 may be so chosen that the area integration of σ_ϕ from a minimum map latitude, ϕ_m, to the pole has a zero value, i.e., so that

$$\int_{\phi_m}^{\pi/2} \frac{\sin \phi_0 - \sin \phi}{1 + \sin \phi} \cos \phi \, d\phi = 0. \tag{8}$$

From [8] it can deduced that

$$1 + \sin \phi_0 = \frac{1 - \sin \phi_m}{\ln 2/(1 + \sin \phi_m)}. \tag{9}$$

If ϕ_m is 65°, ϕ_0 is approximately 72° 13′. North of ϕ_0, σ_ϕ is negative; south of ϕ_0, σ_ϕ is positive.

It is of interest to investigate the arithmetic mean value of σ_ϕ, with the above choice of ϕ_0. This will be

$$|\overline{\sigma_\phi}| = -\frac{2}{1 - \sin \phi_m} \int_{\phi_m}^{\pi/2} \frac{\sin \phi_0 - \sin \phi}{1 + \sin \phi} \cos \phi \, d\phi.$$

$$|\overline{\sigma_\phi}| = 2\left\{\frac{1 - \sin \phi_0}{1 - \sin \phi_m} - \frac{\ln (1 + \sin \phi_0)/2}{\ln (1 + \sin \phi_m)/2}\right\}. \tag{10}$$

If ϕ_m is 65°, $|\overline{\sigma_\phi}|$ has the value of 0.012. Thus the mean scale error for short distances is 1.2%. For longer distances, the mean error would be slightly less.

Alternatively, ϕ_0 may be chosen to minimize the arithmetic mean scale error. With ϕ_0 arbitrary, it may be shown that

$$|\overline{\sigma_\phi}| = \frac{1 + \sin \phi_0}{1 - \sin \phi_m} \ln \frac{(1 + \sin \phi_0)^2}{2(1 + \sin \phi_m)} + \frac{1 - 2 \sin \phi_0 + \sin \phi_m}{1 - \sin \phi_m}. \tag{11}$$

If $|\overline{\sigma_\phi}|$ is to be a minimum, differentiation of [11] yields

$$(1 + \sin \phi_0)^2 = 2(1 + \sin \phi_m). \tag{12}$$

$$|\overline{\sigma_\phi}|_m = \frac{\{(1 + \sin \phi_m)^{\frac{1}{2}} - 2^{\frac{1}{2}}\}^2}{1 - \sin \phi_m}. \tag{13}$$

For $\phi_m = 65°$, this gives $\phi_0 = 72°17'$ and $|\overline{\sigma_\phi}|_m = 0.012$, both very similar to the previous calculations.

4. MEAN SCALE ERRORS OF PROJECTIONS FOR POLAR AREAS

It is not possible to evaluate $\bar{\sigma}_\phi$ (algebraic mean) and $|\overline{\sigma_\phi}|$ (arithmetic mean) analytically for the Lambert projection. For a given choice of standard parallels, however, mean scale errors to various values of ϕ_m can be determined from individual scale errors graphically, or by numerical integration.

In the case of the Ney projection it is necessary to investigate the effects of nonconformality. In terms of polar coordinates, with θ measured counterclockwise from the E–W axis, the magnification at latitude ϕ in the direction θ, m_ϕ^*, becomes

$$[14] \qquad m_\phi^* = m_\phi(\sin^2\theta + \cos^2\theta/L^2)^{\frac{1}{2}}.$$

Since all values of θ are equally probable, the mean effective magnification can be found by integration of [14], resulting in an elliptic integral. If L has a value near unity, it can be shown, using a series expansion, that

$$[15] \qquad \overline{m_\phi^*} \simeq m_\phi(1 + L)/2L.$$

For Ney's specific projection ($\phi_1 = 89°59'58''$, $\phi_2 = 71°$, $L = 0.997375$), it follows that

$$\overline{m_\phi^*} = 1.001316\, m_\phi.$$

Values of m_ϕ were obtained for a true Lambert projection from a table given by Ney (3). For the Lambert and Ney projections (ϕ_1 and ϕ_2 as above), σ_ϕ and σ_ϕ^* were evaluated, multiplied by cos ϕ, and integrated (using Simpson's rule) from 90° to the three latitudes: 65, 64, and 63. This was done since it turned out that Ney's choice of ϕ_1 and ϕ_2 was more appropriate to a ϕ_m of 64° than to the ϕ_m of 65° for which it was designed, and a true Lambert for the same ϕ_1 and ϕ_2 was best suited to a ϕ_m of 63.5°. The mean algebraic and arithmetic scale errors for these projections are given in Table I.

TABLE I

MEAN ALGEBRAIC AND ARITHMETIC SCALE ERRORS, EXPRESSED AS PERCENTAGES, FOR LAMBERT AND NEY PROJECTIONS ($\phi_1 = 89°59'58''$, $\phi_2 = 71°$)

ϕ_m(°)	Lambert		Ney	
	$\bar{\sigma}_\phi$(%)	$\overline{\lvert\sigma_\phi\rvert}$(%)	$\bar{\sigma}_\phi$(%)	$\overline{\lvert\sigma_\phi\rvert}$(%)
65	− 0.31	1.14	− 0.18	1.16
64	− 0.13	1.21	0.00	1.22
63	+ 0.06	1.31	+ 0.20	1.31

Corresponding data for polar stereographic projections are given in Table II; the first set of values, the two columns on the left, refer to a fixed ϕ_0 value of 71°, and the second set of values, the three columns on the right, refer to a ϕ_0 for each ϕ_m chosen to minimize $\overline{\lvert\sigma_\phi\rvert}$. $\bar{\sigma}_\phi$ values are also given and it can be seen that the ϕ_0 values are nearly those that give a zero algebraic mean scale value. In this table eccentricity has been neglected, whereas it is considered in Table I. Computations showed, however, that this neglect in Table II was justified.

Thus it can be seen that, even allowing for an adjustment of ϕ_2 to minimize scale errors, the reduction of mean scale error effected by replacing the standard

TABLE II

MEAN ALGEBRAIC AND ARITHMETIC SCALE ERRORS, EXPRESSED AS PERCENTAGES, FOR POLAR STEREOGRAPHIC PROJECTIONS

$\phi_m(°)$	Fixed ϕ_0 (71°)		Best ϕ_0		
	$\bar{\sigma}_\phi(\%)$	$\overline{\lvert\sigma_\phi\rvert}(\%)$	$\bar{\sigma}_\phi(\%)$	$\overline{\lvert\sigma_\phi\rvert}_m(\%)$	ϕ_0
65	− 0.38	1.24	− 0.03	1.20	72°17′
64	− 0.19	1.32	− 0.04	1.30	71°34′
63	0.00	1.41	− 0.04	1.40	70°51′

polar stereographic by the Ney projection amounts to at most 0.06% for a minimum latitude of 65°, 0.08% at 64°, and 0.10% at 63°. This hardly seems sufficient to justify the introduction of a nonconformal nonstandard projection, with its concomitant mean azimuth error of 0.13%. Ney (3) claims that it is not possible to place the northerly standard parallel exactly at the pole, but it can be seen that this can essentially be done, the latitudes of minimum, unity, and infinite map magnification coinciding. This yields the Polar Stereographic projection, which remains as the best polar chart for aeronautical and meteorological purposes.

Actually, of course, the differences between Ney's projection and a suitable Polar Stereographic projection are very small, as can be seen from Table III, which lists the latitude radii (in inches, for a map scale of 30 nautical miles to the inch) and percentage scale errors, for such projections.

TABLE III

LATITUDE RADII, R_ϕ, IN INCHES, AND SCALE ERRORS, σ_ϕ, AS PERCENTAGES, FOR VARIOUS POLAR PROJECTIONS

$\phi(°)$	Ney		Polar Stereographic			
	$\phi_2 = 71°$		$\phi_0 = 71°$		$\phi_0 = 72.5°$	
	R_ϕ	σ_ϕ*	R_ϕ	σ_ϕ	R_ϕ	σ_ϕ
65	49.713	+ 2.11	49.617	+ 2.05	49.827	+ 2.49
71	37.563	+ 0.13	37.463	0.00	37.621	+ 0.42
74	31.565	− 0.63	31.466	− 0.80	31.599	− 0.38
80	19.677	− 1.68	19.591	− 1.98	19.674	− 1.56
85	9.838	− 2.06	9.778	− 2.54	9.819	− 2.13
88	3.943	− 1.98	3.909	− 2.69	3.925	− 2.28

REFERENCES

1. ADAMS, O. S. General theory of polyconic projections. Special Pub. No. 57, U.S. Coast and Geodetic Survey, Washington. 1934.
2. MACK, S. Z. and SHARP, W. T. R.C.A.F. Nav. Bull. 4: 40. 1952.
3. NEY, C. H. Can. J. Research, F, 27: 269–283. 1949.

NOTE

A COMPENSATED RECIPROCATING LABORATORY SHAKER*

By H. Tessier

Common defects of laboratory shakers designed to produce a violent reciprocal motion include: excessive vibration, belt-slip, discontinuous speed variation, and a tendency for the shaker to migrate. The apparatus described in this note eliminates these defects.

The completed shaker (Fig. 1) consists of two aluminum trays, 18 in. by 18 in. by 7 in. deep, mounted on carriages running on rails. The supporting

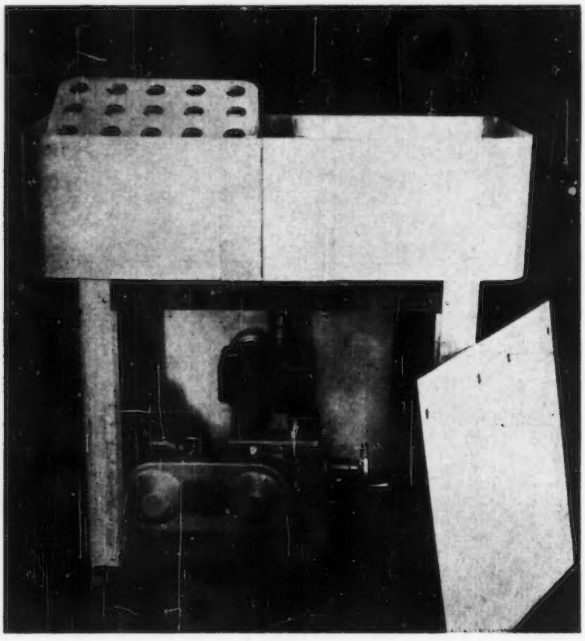

Fig. 1.

frame is of welded $1\frac{1}{4}$ in. iron pipe covered on all sides with an aluminum skirt. One side of the skirt is removable to allow easy access to the drive mechanism. For mobility, the unit is mounted on swivel casters.

*N.R.C. No. 2878.

Samples are held in the trays by snugly fitting fiberboard inserts, cut to accommodate the particular flasks being used (1). Each tray and carriage has a travel of two inches at rates of from 40 to 240 strokes per minute.

Details of the driving mechanism are shown in Fig. 2. Two cams (*A*), set at 180 degrees to one another, are keyed to the vertical drive shaft (*B*) of a ½ h.p.

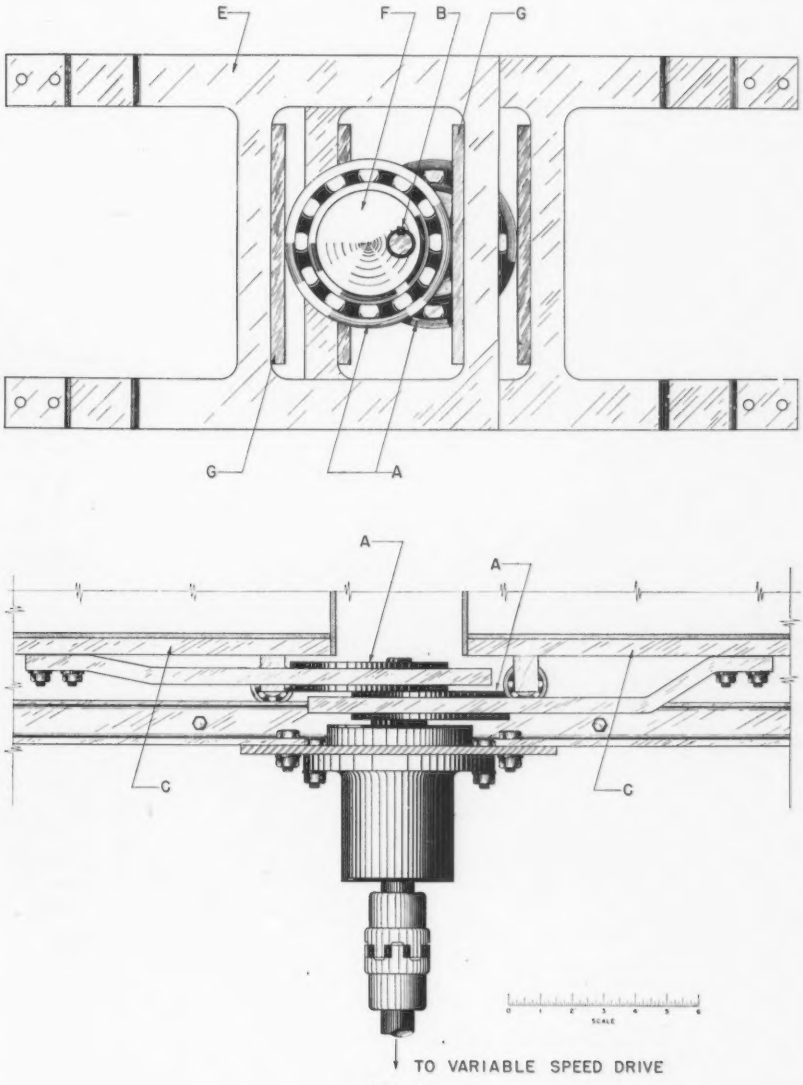

FIG. 2.

worm gear reducer and Tippen variable speed transmission unit. Motion in opposite directions is imparted to the two carriages (*C*) as the eccentrics revolve inside the rectangular frames (*E*). The ball bearing cams (*A*) are 5 in. outside diameter with press-fitted steel inserts (*F*), drilled and keyed to shaft dimensions, one inch off center. The bearing surfaces of the aluminum frames (*E*) are faced with steel strips (*G*) to minimize wear. These facings also permit adjustment of the clearance between cams and frames.

1. WHITE, W. H. Can. J. Research, F, 25: 236-237. 1947.

RECEIVED OCTOBER 9, 1952.
DIVISION OF APPLIED BIOLOGY,
NATIONAL RESEARCH LABORATORIES,
OTTAWA, CANADA.

CANADIAN JOURNAL OF TECHNOLOGY

Notice to Contributors

GENERAL: Manuscripts should be typewritten, double spaced, and the **original and one extra copy** submitted. Style, arrangement, spelling, and abbreviations should conform to the usage of this Journal. Names of all simple compounds, rather than their formulas, should be used in the text. Greek letters or unusual signs should be written plainly or explained by marginal notes. Superscripts and subscripts must be legible and carefully placed. Manuscripts should be carefully checked before being submitted, to reduce the need for changes after the type has been set. If authors require changes to be made after the type is set, they will be charged for changes that are considered to be excessive. **All pages, whether text, figures, or tables, should be numbered.**

ABSTRACT: **An abstract of not more than about 200 words, indicating the scope of the work and the principal findings, is required.**

ILLUSTRATIONS:

(i) *Line Drawings:* All lines should be of sufficient thickness to reproduce well. Drawings should be carefully made with India ink on white drawing paper, blue tracing linen, or co-ordinate paper **ruled in blue only**; any co-ordinate lines that are to appear in the reproduction should be ruled in black ink. Paper ruled in **green, yellow, or red should not be used** unless it is desired to have all the co-ordinate lines show. Lettering and numerals should be neatly done in India ink, preferably with a stencil (**do not use typewriting**) and be of such size that they will be legible and not less than one millimeter in height when reproduced in a cut three inches wide. All experimental points should be carefully drawn with instruments. Illustrations need not be more than two or three times the size of the desired reproduction, but the ratio of height to width should conform with that of the type page. **The original drawings and one set of small but clear photographic copies are to be submitted.**

(ii) *Photographs:* Prints should be made on glossy paper, with strong contrasts; they should be trimmed to remove all extraneous material so that essential features only are shown. Photographs should be submitted **in duplicate**; if they are to be reproduced in groups, one set should be so arranged and mounted on cardboard with rubber cement; the duplicate set should be unmounted.

(iii) *General:* **The author's name, title of paper, and figure number should be written in the lower left hand corner (outside the illustration proper) of the sheets on which the illustrations appear.** Captions should not be written on the illustrations, but typed together at the end of the manuscript. All figures (including each figure of the plates) should be numbered consecutively from 1 up (arabic numerals). **Each figure should be referred to in the text.** If authors desire to alter a cut, they will be charged for the new cut.

TABLES: Each table should be typed on a separate sheet. Titles should be given for all tables, which should be numbered in Roman numerals. Column heads should be brief and textual matter in tables confined to a minimum. **Each table should be referred to in the text.**

REFERENCES: **These should be listed alphabetically by authors' names, numbered in that order, and placed at the end of the paper.** The form of literature citation should be that used in this Journal. **Titles of papers should not be given.** For the references cited inclusive page numbers should be given. **All citations should be checked with the original articles.** Each citation should be referred to in the text by means of the key number.

REPRINTS: A total of 50 reprints of each paper, without covers, are supplied free to the authors. Additional copies will be supplied according to a prescribed schedule of charges. On request, covers can be supplied at cost.

Approximate charges for reprints may be calculated from the number of printed pages, obtained by multiplying by 0.6 the number of manuscript pages (double-spaced typewritten sheets, 8½ in. by 11 in.) and making allowance for space occupied by line drawings and half-tones (not inserts). The cost per page is tabulated at the back of the reprint request form sent with the galley.

Contents

Printed in Canada *by* University of Toronto Press